The effect of post-tensioning on the behavior of small-scale 3D-printed concrete beams

Damon BOLHASSANI[*], Fahimeh YAVARTANOO, Javier TAPIA, Masoud AKBARZADEH[a],
Maximilian E. ORORBIA[a], Hua CHAI[a], Yefan ZHI[a], Mylene BERNARD[b], Leon TROUSSET[b],
Karolina PAJAK[b], Blaise WALIGUN[b], Paul KASSABIAN[b]

[*] ABC Lab, Spitzer School of Architecture, The City College of New York (CCNY), New York, USA
[*] mbolhassani@ccny.cuny.edu

[a] Polyhedral Structures Laboratory, Weitzman School of Design, University of Pennsylvania, Philadelphia, USA
[b] SIKA, Zurich, Switzerland
[c] Simpson, Gumpertz, & Heger (SGH), Boston, USA

Abstract

Producing large-scale 3D-printed elements in a continuous session is often impractical, highlighting the need for prefabrication of smaller segments that can subsequently be assembled. However, the lack of perfect bonds between joints may cause a lower strength than conventionally cast concrete. Hence, it is crucial to evaluate the behavior of members produced by the segmented assembly approach with appropriate reinforcement mechanisms to enhance their integrity. This study outlines an experimental program aimed at evaluating the structural behavior of small-scale post-tensioned 3D-printed concrete beams composed of three segments. Initially, three specimens were employed to examine material behavior. The findings demonstrate a compressive strength of approximately 25 MPa and varying tensile strengths ranging from 1.82 MPa to 1.89 MPa, depending on specimen orientation. In the next step, flexural strength tests were conducted to evaluate the structural performance of two 3D-printed concrete beams under diverse conditions. The first beam, subjected to a 3-point bending configuration and a post-tensioning force of 133.44 kN, exhibited a maximum load of 75.7 kN at a displacement of 35 mm. The observed brittle behavior, characterized by explosive compressive failure, suggests a potential excess in the applied post-tensioning force. Conversely, the second beam, tested under a 4-point bending configuration with an ungrouted condition and a post-tensioning force of 66.7 kN, displayed a larger maximum load of 87.6 kN at a displacement of 38 mm compared to the first beam. Despite maintaining a compressive failure mode, this beam exhibited a nonexplosive behavior with ductility characteristics. Notably, significant damage to the plastic cover was observed due to a strong interaction between the cable and the void. The observations in this study emphasize the critical necessity of considering the interplay between post-tensioning, grouting, and cable-induced effects in the design of 3D-printed concrete beams.

Keywords: Experimental testing, post-tensioning, periodic anticlastic funicular beam, 3D concrete printing

1. Introduction

The carbon emissions generated by the construction industry urge the adoption of eco-friendly practices to minimize environmental impact. In response, researchers and professionals are actively exploring sustainable materials and technologies to construct greener and more environmentally responsible structures (Nilimaa [1]). Among these advancements, 3D concrete printing has emerged as a transformative

technology (Khan et al. [2], Wangler et al. [3]) that enhances construction efficiency by optimizing material usage and minimizing waste. Precise layer-by-layer concrete deposition notably reduces the need for formwork and minimizes material waste, consequently contributing to a significant decrease in carbon emissions linked to concrete production. Equally critical in advancing towards sustainability is topology optimization. This methodology ingeniously addresses structural efficiency by mathematically determining the most material-efficient configurations for specific loads and constraints. Applied to 3D concrete printing, topology optimization allows for the creation of intricate geometries that harness material strength more effectively (Vantyghem et al. [4]). This not only optimizes the performance of concrete elements but simultaneously reduces material consumption. By enabling the generation of lightweight yet structurally robust designs, topology optimization substantially minimizes the use of materials, leading to fewer resources consumed during both production and transportation. While these innovative techniques hold immense potential for reducing carbon emissions and enhancing sustainability, it is crucial to acknowledge that, at the current stage, ensuring the safety of 3D-printed structures demands rigorous structural design and analysis. While 3D concrete printing offers novel possibilities, the need for careful engineering oversight remains paramount. Adequate consideration of factors such as longitudinal and horizontal reinforcement is essential to ensure the structural integrity and stability of the printed components (Gebhard et al. [5]). Additionally, the anisotropy resulting from the layered nature of 3D printing introduces complexities that require meticulous evaluation (Wolfs et al. [6]). As the construction industry seeks to harness the benefits of these advancements, it must navigate the balance between innovation and ensuring safety to fully realize the potential of 3D concrete printing in sustainable construction practices. Addressing the need for structural integrity in 3D-printed concrete, a critical consideration is the incorporation of longitudinal reinforcements. Notably, two prominent reinforcement methods have been extensively explored in the literature: conventional steel reinforcements and prestressing reinforcements, primarily in the form of post-tensioning (Gebhard et al. [5]). Conventional steel bars, commonly used in traditional construction, can be strategically positioned within the voids of the print and subsequently grouted. This approach provides enhanced strength to the structure. However, it is essential to acknowledge that incorporating stiff steel bars can potentially limit the geometric flexibility of the printed element due to the fixed positions of the bars. In contrast, post-tensioning offers a distinct advantage in terms of geometric flexibility. Post-tensioning reinforcements, whether grouted or left ungrouted, provide an opportunity for adjusting the tensioning force after the concrete has cured. This adjustability enables a more refined control over the element's behavior and allows for optimization based on the specific load conditions. This paper presents the application of post-tensioning to a 3D-printed concrete beam, specifically within a basic cross-sectional framework comprising three modular 3D-printed concrete segments. This investigation involves systematically altering key parameters, including segment junction configurations, post-tensioning duct grouting options, and post-tensioning force magnitudes. In the subsequent phase, flexural bending tests, utilizing both 3-point and 4-point configurations, were performed on three modular 3D-printed concrete beams. These tests aimed to assess the structural behavior of the beams under the most critical conditions.

2. Experimental program

The experimental program aimed to investigate the effect of post-tensioning on the behavior of small-scale 3D-printed concrete beams. In total, nine specimens served dual purposes in both assembling the post-tensioned beam and conducting the compressive and tensile splitting tests.

2.1. Specimen preparation

The choice of shape and geometry for the concrete beam was guided by practical considerations associated with the 3D printing process and the unique challenges posed by the construction of large-scale 3D-printed elements. Large-scale 3D-printed elements cannot be produced in a single continuous session, necessitating the prefabrication of individual segments that would later be assembled. Therefore, in response to the limitations of current 3D printing technology, a segmented assembly approach was adopted. This methodology aligns with the constraints and capabilities of current 3D printing technology. The concrete beam used in this study consists of three identical segments, each approximately 36 cm in length, and a cross-section measuring 15 cm by 20 cm as visually depicted in Figure 1. The geometry of each segment deviates from traditionally cast concrete beams due to the 3D-printing process introducing a partial discontinuity along the middle of the cross-section. Consequently, the chosen beam roughly resembles a U section, in contrast to regular concrete beams that exhibit uniformity without layers or discontinuities. This distinctive geometry is a result of the layering inherent in the 3D printing process and the printing path chosen for the specimen.
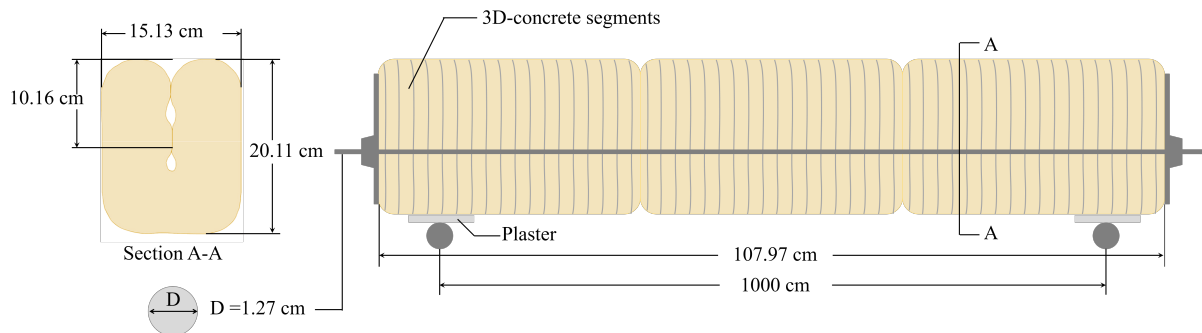
Figure 1: 3-D printed concrete specimen

2.2. Material properties

The fundamental component of this experimental investigation, the 3D printing material, along with the meticulous printing process of the specimens, has been generously supplied by Sika, a prominent leader in construction technology, renowned for its proprietary nature and commitment to superior quality. The strategic decision, covering both the supply of the 3D printing material and the meticulous printing process executed by Sika, exemplifies a dedication to advancing technological frontiers in the realm of 3D-printed construction. To determine the mechanical properties of the 3D-printed concrete specimens, two testing machines were employed, which are standardized testing methods as widely documented in technical literature [7, 8, 9, 10, 11, 12]). The Instron 5500 (maximum capacity of 2,225 kN) facilitated compressive and splitting tensile tests, while the Instron 5582 (maximum capacity of 100 kN) conducted 3-point and 4-point bending tests. According to the compressive test results, the specimen could resist a maximum load of 1380 kN, corresponding to a compressive strength of 25 MPa, which is an acceptable strength for structural design. Splitting tensile strength tests have been conducted in two orientations. In Orientation 1, the failure load was observed at 98.86 kN, resulting in a splitting tensile strength of 1.82 MPa. In Orientation 2, the failure load was slightly lower at 91.2 kN, but the recorded strength was higher at 1.89 MPa. A couple of challenges were encountered in replicating the splitting tensile test setup, according to the ASTM standard, C-496 due to the size, weight, and geometry of the specimens. Inherently, as a result of 3D-printing concrete, a form of additive manufacturing, the layers are integral to the process. Consequently, during the printing of the specimen, the layers at the base protruded outward due to the self-weight of the specimen, posing difficulties in ensuring consistent contact between

the load-applying rod and the 3D-printed concrete. To address this issue, plaster of Paris was uniformly applied, to distribute the load evenly across the uneven layers and minimize stress concentration. The ASTM standard C-496 determines the splitting tensile strength of cylindrical specimens using the equation $T = 2P/(\pi l d)$, where, T is the tensile strength, P is the maximum applied load, l is length, d is the diameter, and the reduction factor of $2/\pi$ is applied to account for the biaxial state of stresses induced by the forces in the test. In this formulation, approximately $2/\pi$ of the cross-sectional area is considered to resist tension, while the remaining resists compression. In response to the challenges posed by the intricate geometry of the specimens, the strength was calculated by $T = P/(l h)$, where l and h are the length of concrete directly under the load and the height of the specimen, respectively. The elimination of the reduction factor of $2/\pi$ is motivated by the intention to approximate the upper bound of the tensile strength by assuming that the entire cross-sectional area contributes to resisting tension.

3.   Flexural strength test

The geometric flexibility of 3D-printed concrete is a key consideration, but it presents challenges in terms of reinforcement. Traditional rebars, for example, can only navigate through straight voids, limiting their application. To overcome this limitation, post-tensioning was chosen as the preferred method of reinforcement. The flexibility of a cable allows it to navigate through voids, providing structural strength while accommodating geometric intricacies. A steel cable with a cross-sectional area of 126.61 mm2 was post-tensioned at the force of 133.44 kN and 66.72 kN for conducting flexural strength tests under 3-point and 4-point bending loads, respectively. The post-tensioning process was executed by the POWER TEAM Post Tensioning Pump, a high-performance device equipped with a two-speed mechanism and an adjustable pressure relief valve spanning 1000 psi (6.9 MPa) to 10,000 psi (68.9 MPa), which ensures meticulous precision during post-tensioning operations. The control valve, with "advance," "hold," and "return" positions, granted precise control of prestressing force in the beam. Noteworthy is the inclusion of a remote motor control hand switch with a 10' cord, enhancing operational flexibility. With a power capacity of 1/2HP, 25 amps, and 12,000 rpm, the POWER TEAM pump exemplifies robust engineering and reliability in executing post-tensioning protocols. At the core of the advanced post-tensioning system employed is the meticulously designed AMSYSCO Encapsulated PT System, providing unparalleled corrosion protection. The steel strand (cable) undergoes a multi-step process, starting with a specialized high-quality anti-corrosion PT coating (grease). High-density plastic sheathing, applied using state-of-the-art extrusion technology, ensures uniform protection against environmental elements. Each anchorage is fully encapsulated in an extruded jacket of high-density polyethylene, adding an extra layer of defense. The anchor/strand connection is fortified with a tightly sealed plastic sleeve, and a grease-filled cap on the tendon ends prevents moisture intrusion, enhancing the long-term viability of the post-tensioning system. This meticulous attention to detail in the design and execution of the AMSYSCO Encapsulated PT System significantly contributes to the reliability and durability of the post-tensioning process in the experimentation. The flexural strength test was conducted to evaluate the structural performance of 3D-printed concrete beams across two specific scenarios of 3-point and 4-point bending tests. Due to the small size of the beam prototype and the capacity limitations of the hydraulic jack, the 3-point bending test was assumed to be more appropriate initially and conducted as the first scenario. The 3-point bending test, with its concentrated load application at the midspan, allowed for a straightforward assessment of the beam's maximum flexural strength. However, during testing, the beam experienced catastrophic failure (explosion) under the concentrated load, highlighting the need for a method that could distribute the load more evenly and mitigate such failure risks. Consequently, the 4-point bending test was conducted to provide a more uniform stress distribution over the beam. The advantage of conducting a 4-point bending test lies in its ability to create a constant bending moment between the two loading points, offering a more accurate representation of the pure flexural behavior of

the beam over an extended region and reducing the likelihood of localized failure. Therefore the second scenario was dedicated to the 4-point bending test.

3.1.   Scenario 1: 3-point bending test

In the first scenario indicated in Figure 2a, 3-point bending configuration was utilized, and a post-tensioning force of 30 kip (133.44 kN) was applied. The force-displacement Figure 2b curve revealed a maximum load of 75.7 kN at a displacement of 35 mm. The mode of failure was characterized as an explosive compressive failure, suggesting a potential excess in the applied post-tensioning force (133.44 kN). Furthermore, the force-displacement curve identified the first crack load at 24 kN, leading to the delamination of layers at midspan in the beam. It is crucial to note that the corresponding first-crack strength does not represent the splitting tensile strength of the material but rather signifies the bond strength at the interfaces between layers, measured at 1.66 MPa on the stress-strain curve. The initiation of the crack directly under the load and strain gauge introduced uncertainty in strain readings, impacting the determination of the modulus of elasticity. This crack initiation serves as a point of structural weakness, highlighting the anisotropic behavior inherent in 3D-printed concrete and the delamination of layers. Determining whether the layer interface bond strength is lower than the splitting tensile strength, considering the upper bounds of 1.82 and 1.89 MPa obtained by splitting tensile test, poses a challenge. Nevertheless, a reasonable assertion can be made that anisotropic behavior is minimal, although potential variations may exist based on the specific printing quality.
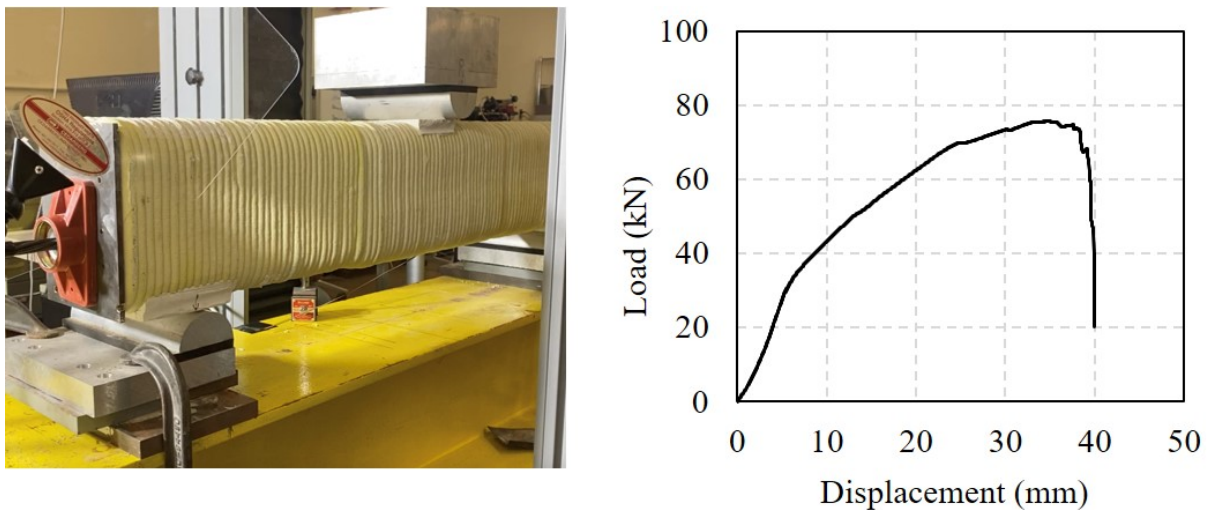
Figure 2: Experimental setup and the force-displacement curve under 3-point bending load

The cable used in this scenario was coated with a high-quality anti-corrosion PT coating (grease) and enclosed in high-density plastic sheathing manufactured through an advanced extrusion process. Additionally, a tightly sealed plastic sleeve at the anchor/strand connection provided further protection. Visual examination suggested that the cable within the void did not yield, emphasizing the significance of the interaction between the cable and the void. The plastic cover of the cable sustained damage, resulting in observed grease leakage.
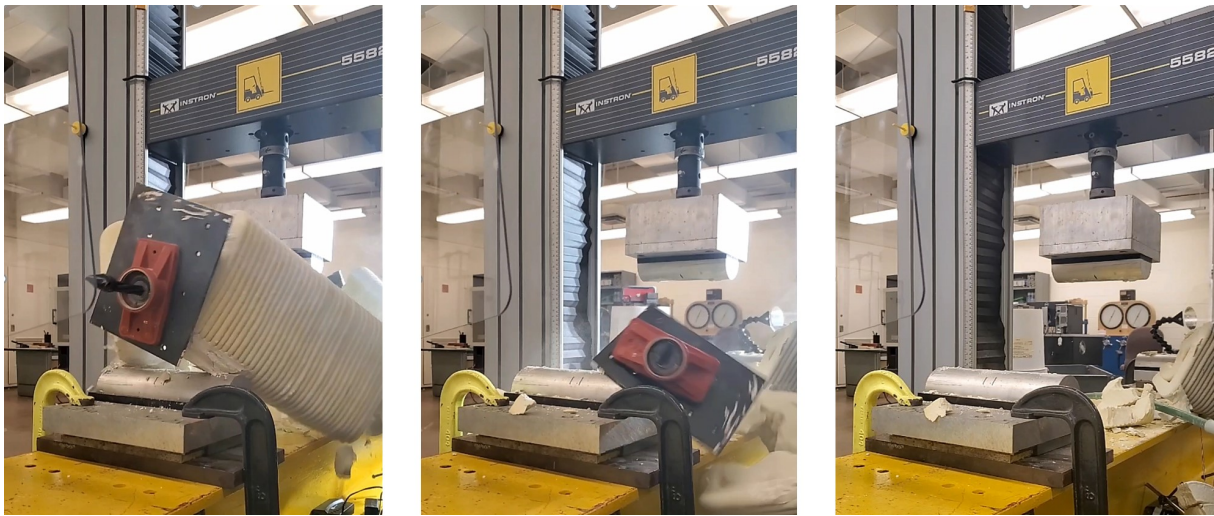
Figure 3: Failure mechanism under 3-point bending load (explosive compressive failure)

3.2. Scenario 2: 4-point bending test

In the investigation of the beam subjected to 15 kip (66.7 kN) post-tensioning, 4-point bending (Figure 4a), and an ungrouted condition, the force-displacement curve (Figure 4b) exhibited a maximum load of 87.6 kN with a corresponding displacement of 38 mm. Notably, the first crack emerged at a load of 20 kN, resulting in a first-crack strength of 1.17 MPa, a value notably lower than the preceding tensile strength results. While the mode of failure retained a compressive nature, the behavior was nonexplosive and demonstrated characteristics of ductility. However, the plastic cover displayed substantial damage, indicative of a significant interaction between the cable and the void. Moreover, this interaction was so pronounced that it led to the formation of irregular transverse cracks an occurrence uncommon in traditionally casted reinforced concrete beams. These transverse cracks may be attributed to unbonded surfaces between segments, potentially resulting from stress concentration. Yet, upon closer examination, these cracks appear to be influenced by the cable. Evidence for this lies in the presence of transverse cracks beneath the beam as well. The cable's response to the load may be generating an uplifting force, forcefully causing the specimen to split open, particularly in areas where the bond in the "U-section" is relatively insignificant. This intricate interplay between post-tensioning, the absence of grouting, and the consequential cable-induced effects on the specimen's behavior underscores the importance of considering multiple factors in the design and analysis of 3D-printed concrete structures subjected to complex loading conditions.

4. Conclusion

This study aimed to investigate the structural behavior of 3D-printed concrete structures with complex geometries. Nine specimens were fabricated using SIKA 3D-printing concrete material. Material testing revealed satisfactory compressive strength properties suitable for construction purposes. Variations in tensile strength in different orientations were observed, consistent with the expected anisotropic nature of 3D-printed concrete. Subsequently, flexural strength tests were conducted in both 3-point and 4-point bending configurations to evaluate the structural performance of the beams. The results underscored the importance of post-tensioning in enhancing structural integrity. In the 3-point bending test, an abrupt and explosive failure mode was observed, highlighting the intricate interplay between post-tensioning forces and geometric complexities. The appearance of transverse cracks, uncommon in traditional re-
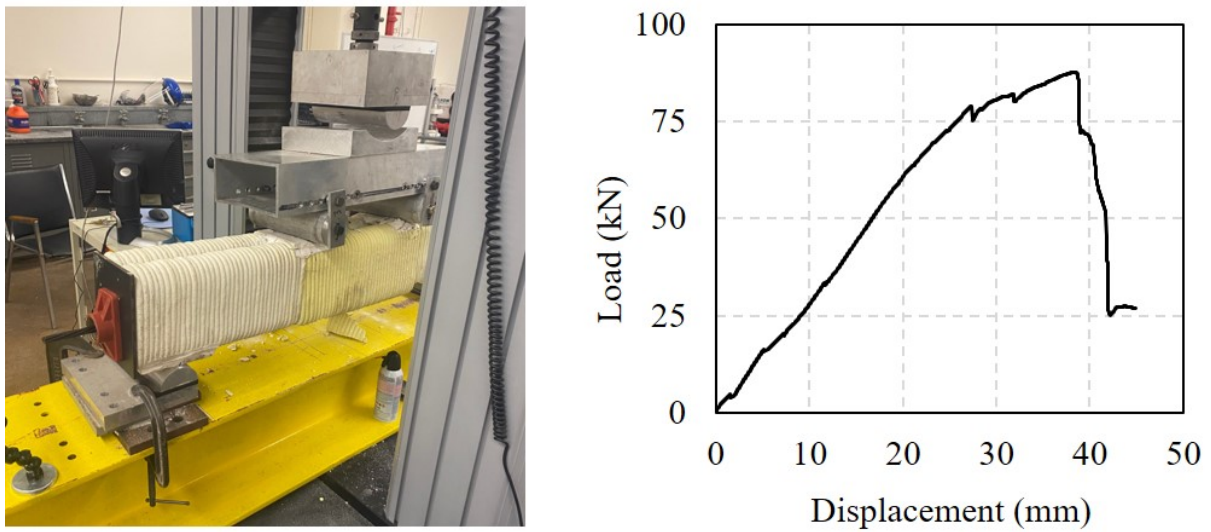
Figure 4: Experimental setup and the force-displacement curve under 4-point bending load

Figure 5: Failure mechanism under 4-point bending load

inforced concrete, emphasized the challenges posed by cable-void interactions. Conversely, the 4-point bending test exhibited a non-explosive failure mode and more ductile behavior, providing insights into the impact of post-tensioning and the absence of grouting on specimen response. The formation of irregular transverse cracks, attributed to cable-induced effects, underscores the necessity for comprehensive consideration of these factors in the design and analysis of 3D-printed concrete structures. It is important to note that the results obtained from the 3-point and 4-point bending tests served as a foundation for validating and refining the numerical model of 3D-printed concrete beams, which will subsequently analyze a broader range of cases with different sizes and configurations. This approach allows for a more extensive parametric study to be performed numerically. Moreover, these results can contribute to advancing 3D-printed concrete technology and its application in the construction industry.

Acknowledgments

References

[1] J. Nilimaa, "Smart materials and technologies for sustainable concrete construction," *Developments in the Built Environment*, p. 100 177, 2023.

[2] S. A. Khan, M. Koç, and S. G. Al-Ghamdi, "Sustainability assessment, potentials and challenges of 3d printed concrete structures: A systematic review for built environmental applications," *Journal of Cleaner Production*, vol. 303, p. 127 027, 2021.

[3] T. Wangler *et al.*, "Digital concrete: Opportunities and challenges," *Rilem technical letters*, vol. 1, no. 1, pp. 67–75, 2017.

[4] G. Vantyghem, W. De Corte, E. Shakour, and O. Amir, "3d printing of a post-tensioned concrete girder designed by topology optimization," *Automation in Construction*, vol. 112, p. 103 084, 2020.

[5] L. Gebhard, J. Mata-Falcón, A. Anton, B. Dillenburger, and W. Kaufmann, "Structural behaviour of 3d printed concrete beams with various reinforcement strategies," *Engineering Structures*, vol. 240, p. 112 380, 2021.

[6] R. Wolfs, F. Bos, and T. Salet, "Hardened properties of 3d printed concrete: The influence of process parameters on interlayer adhesion," *Cement and Concrete Research*, vol. 119, pp. 132–140, 2019.

[7] A. Hamid, M. Bolhassani, A. Turner, E. Minaie, and F. Moon, "Mechanical properties of ungrouted and grouted concrete masonry assemblages," in *12th Canadian Masonry Symposium Vancouver, British Columbia, June*, 2013, pp. 2–5.

[8] A. R. Khaloo, A. G. Vayghan, and M. Bolhassani, "Mechanical and microstructural properties of cement paste incorporating nano silica particles with various specific surface areas," *Key Engineering Materials*, vol. 478, pp. 19–24, 2011.

[9] M. Bolhassani, M. Akbarzadeh, M. Mahnia, and R. Taherian, "On structural behavior of a funicular concrete polyhedral frame designed by 3d graphic statics," in *Structures*, Elsevier, vol. 14, 2018, pp. 56–68.

[10] F. Yavartanoo, T. H.-K. Kang, T.-U. Ha, W.-Y. Lim, and S.-G. Hong, "Restoration of mireuksaji stone pagoda: Evaluation of reinforced granite members with titanium bars," *Journal of Performance of Constructed Facilities*, vol. 34, no. 4, p. 04 020 046, 2020.

[11] F. Yavartanoo, T. H.-K. Kang, S. Jeon, and S.-G. Hong, "Investigation of material and structural performance of mireuksaji stone pagoda," *Journal of Performance of Constructed Facilities*, vol. 33, no. 6, p. 04 019 059, 2019.

[12] F. Yavartanoo, T. H.-K. Kang, T.-U. Ha, W.-Y. Lim, and S.-G. Hong, "Flexural behavior of reinforced granite members with titanium bars," *Journal of Performance of Constructed Facilities*, vol. 35, no. 5, p. 04 021 047, 2021.